Microstructural and Mechanical Characterization of Actively Brazed Alumina Tensile Specimens

Alumina wetting and tensile specimens are brazed with Au-Ni-Mo-V active brazing alloys

BY F. M. HOSKING, C. H. CADDEN, N.Y.C. YANG, S. J. GLASS, J. J. STEPHENS, P. T. VIANCO AND C. A. WALKER

ABSTRACT. Alumina (94 and 99.8% grade compositions) was brazed directly to itself with gold-based active brazing alloys (ABAs) containing nominally 1, 2 or 3 wt-% vanadium. The effects of brazing conditions on the joint properties were investigated. Wetting behavior, interfacial reactions, microstructure, hermeticity and tensile strength were determined. Wetting was generally fair to good for the ABA and base-material combinations. Microanalysis identified a discontinuous reaction product at the alumina-braze interface as an Al-V-O spinel-type phase. Tensile strength of the 94% alumina specimens was generally not sensitive to the vanadium concentration and consistent within an 85–105 MPa range. The tensile data for the 99.8% alumina specimens, however, had significantly greater variability, with values ranging from 25 to 95 MPa. The highest value was obtained for the samples brazed with the filler metal containing 3 wt-% vanadium. Fractures occurred either along the braze-alumina interface for the 99.8% alumina specimens or through the alumina piece with the 94% alumina samples.

Introduction

The development of "active" brazing as a reliable joining technology for engineered ceramics (ceramic-to-ceramic and metal-to-ceramic joints) requires a fundamental understanding of the interfacial and bulk microstructural features of the brazement. In general, the mechanical behavior of any brazed assembly is intrinsically dependent on these features, as well as the residual stress state in the joint. However, when joints involve a ceramic substrate with high modulus and limited ductility (compared to metals), interfacial structures are particularly important in determining mechanical behavior of the bonded assembly. By correlating the joint structure with mechanical strength, a relationship can be developed that provides the basis for engineering critical braze joints with properties that satisfy explicit processing and service requirements.

Active braze alloys (ABAs) have been developed as a means to directly wet a ceramic, without the need for metallization of its surface (Refs. 1–11). Since the ABA's ability to work depends on the chemical reaction(s) that occurs between the active element(s) in the braze and the ceramic, a fundamental understanding of how the brazing parameters affect the interfacial reaction kinetics is an important step toward controlling and optimizing the ABA process. Once this is achieved and the braze chemistry, microstructures and properties are quantified, structural responses can be predicted.

Early active alloy systems primarily utilized titanium as the active component. The resulting filler metals were limited to processing in either vacuum or inert atmospheres since titanium forms hydrides in reactive, hydrogen atmospheres. Recently, a new family of alloys was developed that is more compatible with hydrogen, employing vanadium as the active constituent. These second-generation ABAs expand the application of "active brazing technology" to areas where the preferred, or required, furnace atmosphere is dry hydrogen, such as in the fabrication of high-voltage tube assemblies. Since these vanadium-containing alloys are relatively new, interfacial and microstructural data for prototype ceramic joints are limited. Such braze joints have yielded generally acceptable hermeticity and tensile strength, but the reaction product(s) responsible for adhesion, a necessary condition for realizing the required joint properties, is not well understood.

The present work examined the materials and processing requirements associated with actively brazing 94 and 99.8 wt-% alumina with a vanadium-containing ABA. The braze composition is based on a modified AWS BAu-4 chemistry (82Au-18Ni, wt-%), with 0.75% Mo and three different vanadium concentrations (1 to 3 wt-%). Wetting behavior, interfacial reactions, microstructure and tensile button strength were determined. The results are reported and discussed below.

KEY WORDS

Alumina
Brazing
Gold-Based Alloys
Active Brazing
Ceramic-to-Ceramic
Metal-to-Ceramic

Experimental Conditions and Test Criteria

Materials and Test Specimens

The base materials consisted of two grades of alumina ceramic, 94 and 99.8 wt-% (92 and 99.8 vol-%), procured from WESGO Ceramics, Belmont, Calif., and Coors Ceramics, Golden, Colo., re-

F. M. HOSKING, C. H. CADDEN, N.Y.C. YANG, S. J. GLASS, J. J. STEPHENS, P. T. VIANCO and C. A. WALKER are with Sandia Corp., a Lockheed Martin Co., Albuquerque, N.Mex.

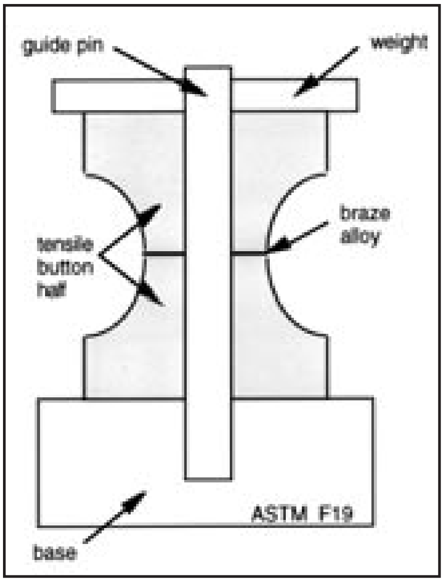

Fig. 1 — Cross-sectional schematic of a cylindrical ASTM F19 ceramic tensile button with braze fixturing.

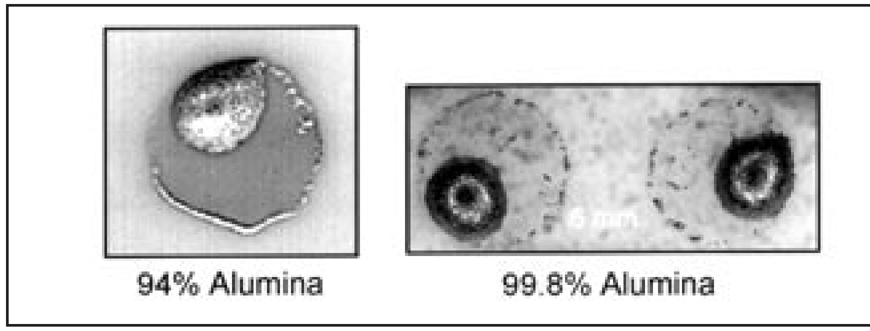

Fig. 2 — Typical wetting behavior of Au-Ni-Mo-2V filler metal on 94% (left) and 99.8% (right) Al_2O_3 substrates.

spectively. The 94% composition contains a glassy phase consisting primarily of silicon, aluminum, magnesium and calcium oxides that are deliberately added to the Al_2O_3 as a sintering aid. Both ceramics were air fired at 1575°C (2867°F) for 2 h prior to brazing in accordance with a manufacturer's recommendations (Ref. 1).

The ABA compositions were based on the Au-Ni-Mo-V quaternary system; their compositions are listed in Table 1. The nominal vanadium concentration was 1, 2 or 3 wt-%. Braze preforms were fabricated from 0.076-mm (0.003-in.) thick foil stock obtained from WESGO, Inc. The melting temperature range for these three alloys, reported by the manufacturer, is 955–970°C (1751–1778°F).

Braze properties were determined using two different test geometries. The first utilized a flat ceramic surface and a 6-mm (0.25-in.) diameter braze alloy disk to quantify wetting behavior. The test was based on the area-of-spread or sessile drop approach (Refs. 12, 13). The second test geometry was based on the ASTM F19-64 (Ref. 14) tension tensile button specimen for evaluating the tensile strength of brazed ceramics, shown schematically in Fig. 1. Seven F19 tensile specimens were fabricated per brazing condition.

Brazing Conditions

Wetting and mechanical test specimens were heated to 1000 or 1020°C (1832 or 1868°F) with 0.076-mm (0.003-in.) thick braze preforms in a slightly positive-pressure, dry-hydrogen atmosphere having a dew point of approximately –60°C. Tensile specimens were brazed in a fixture designed to maintain axial alignment. A small weight was placed on top of the ceramic/braze foil/ceramic assembly to produce a consistent bonding pressure of 7 kPa (1.0 lb/in.^{2}).

Two temperature/time brazing regimes were investigated. The only difference between the two cycles was the peak temperature. Otherwise, the thermal ramp times were the same. The nominal profile was as follows:

- Heating from ambient to 925°C at 10°C/min.
- Soaking at 925°C for 10 min.
- Heating from 925°C to peak temperature (1000 or 1020°C) at 5°C/min.
- Soaking at peak temperature for 5 min.
- Furnace cooling from peak temperature to 800°C at 15°C/min.
- Continued furnace cooling from 800 to 400°C at 10°C/min.
- Final cooling to ambient temperature at 5°C/min.

The furnace temperature was controlled with thermocouples located next to the wetting substrates or on the fixtured tensile specimens. Orientation in the furnace (top vs. bottom) was maintained for each tensile sample.

Analyses and Measured Responses

The brazed samples were evaluated for braze wettability, hermeticity and tensile strength. The ASTM F19 tensile specimens were helium-leak checked, dimensionally inspected for part axial alignment and tested in tension mode. The leak tests were performed with an Alcatel ASM-10 helium leak detector. The machine's leak rate was calibrated with a standard helium leak. Tests were conducted with technical-grade helium. The annular region of the test specimen was evacuated and helium was introduced around the outer fillet. If no leaks were detected, the test scale was changed to increasing helium sensitivity levels until the machine limit was reached. If a leak was detected, the leak range was quantified. The percentage of no detectable leaks (NDL) per data set was then calculated. Specimen alignment measurements were conducted with an optical profilometer. Axial and radial positioning, including tilt and bore concentricity, were measured.

Table 1 — Active Brazing Alloy Composition (wt-%)

Alloy	Au	Ni	Mo	V	Melting Range (°C)
Baseline	82.0	18.0	—	—	955
1	82.8	15.6	0.7	1.0	949–958
2	81.8	15.7	0.7	1.8	940–960
3	80.9	15.5	0.7	2.9	953–958

Room-temperature tensile tests were performed with a hydraulic load frame in displacement control mode at a test rate of 0.0076 mm/s (0.0003 in./s). Universal collated fixturing was used to align the test specimens in the grips during tension testing. The top half of each specimen, as determined by its orientation in the brazing furnace, was loaded in the upper grip of the test machine. Tensile results were compared to baseline values obtained from a control set of metallized and nickel-plated (Mo-Mn-Ni process) 94% alumina tensile button specimens that were brazed with conventional 82Au-18Ni filler metal(AWS BAu-4) at 1000°C.

Finally, one brazed tensile specimen from each processing group was selected for microstructural analyses. A sample was cross sectioned, mounted and metallographically polished for examination using both optical and scanning electron microscopy. Additionally, thin foils were prepared for transmission electron microscopy.

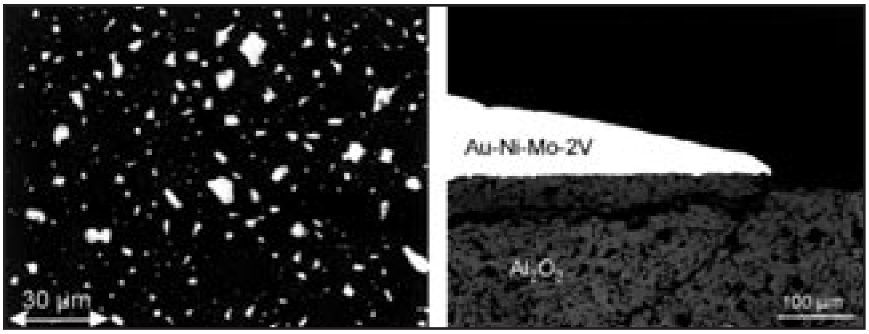

Fig. 3 — Surface (left) and cross section (right) views of 94% Al_2O_3/Au-Ni-Mo-2V wetting sample.

Table 2 — Free Energy Change for Possible Oxide Reduction Reactions at 1020°C

Chemical Reaction	G (kJ/mol)
$Al_2O_3 + 2V \rightarrow V_2O_3 + 2Al$	331
$Al_2O_3 + 3V \rightarrow VO + 2Al$	262
$Al_2O_3 + 3/2Mo \rightarrow 3/2MoO_2 + 2Al$	726
$SiO_2 + 2V \rightarrow 2VO + Si$	9
$3/2\ SiO_2 + 2V \rightarrow V_2O_3 + 3/2\ Si$	49
$SiO_2 + Mo \rightarrow MoO_2 + Si$	287

where $G_T = \Delta H_{298} + \int \Delta C_p dT - T\Delta S_{298} - T\int (\Delta C_p/T)\, dT$, integrated from 298 to 1293 K

Experimental Results

Wetting Behavior

The wetting trials indicated the braze preform retracted from its original disc shape to form an irregular sessile drop, with braze remnants over the initial preform perimeter — Fig. 2. Contact angles of the main droplet generally varied between 30 and 45 deg. Higher values were also observed, although they were not as common. The general experimental observation was that the wetting behavior on both alumina materials was relatively consistent from one braze composition to the next.

Contact angle along the outer edge of the braze droplet on the alumina substrate is an excellent indicator of braze wettability. If its value is 45 deg or less, wettability is usually considered acceptable. Wetting behavior improves as the angle decreases. Ideal wetting occurs when the contact angle approaches zero.

Based on the limited wetting tests conducted, there did not appear to be any significant differences in general wetting between the three braze alloys, although the 1% vanadium composition did yield a larger contact-angle range, with some contact-angle values as high as 60 deg. The alloys containing 2 and 3% vanadium gave more consistent wetting results but did not form substantially lower angles. The average wetting angle, however, was similar for both alloys. There also appeared to be more braze material on the de-wetted 94% alumina surfaces as the vanadium concentration was increased.

Surface analysis on de-wetted 94% alumina surfaces was conducted using scanning electron microscopy. The analytical results revealed braze material concentrated along the exposed glassy phase in the alumina grain boundaries. Bridging occurred occasionally between the smaller braze "islands," forming longer braze segments — Fig. 3. In these de-wetted areas, while the braze material was occasionally found situated on the surface of alumina grains, there was a definite preference for the metal to be retained at grain boundary areas.

Thermodynamic calculations were performed to determine probable reaction products between the ceramic and braze materials. Gibbs free-energy values were calculated for simple alumina and silica reactions with vanadium and molybdenum at 1020°C. In all cases, the resulting oxide reduction and interfacial reaction yield an energetically unfavorable (positive) free-energy value (Table 2). For example, the Gibbs free-energy change for the reaction between alumina and vanadium free energy is 260 kJ/mol or greater. The closest to a negative free-energy change is for the reaction between silica and vanadium, a 9 kJ/mol value. The smaller free-energy change also corresponds to the experimentally observed wetting by each alloy to the 94% alumina glassy phase, which contains a significant amount of silica. The computations suggest more complex reactions occur between the active braze constituent and the surface oxide, particularly for the 99.8% alumina specimens.

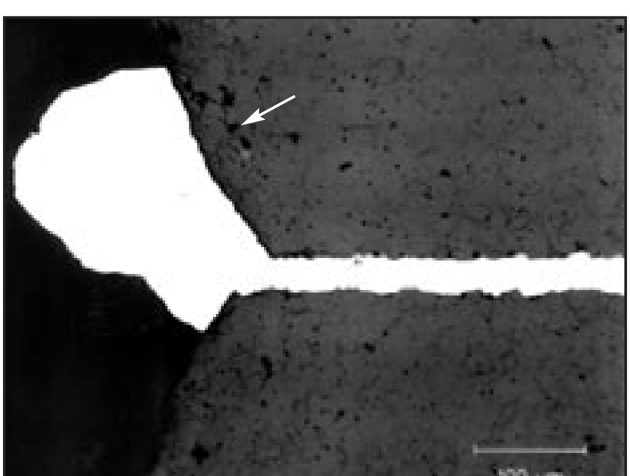

Fig. 4 — A "braze ball" formed at the free surface of a 99.8% alumina F19 braze joint as a result of the localized expulsion of filler metal. Note cracks in the ceramic substrate (arrow).

Fig. 5 — Cross section of a 94% Al_2O_3 sample brazed with the Au-Ni-Mo-2V alloy at 1000°C.

Table 3 — Tensile Strength of Brazed ASTM F19 Alumina Tensile Specimens

Alumina Grade (%)	Braze Composition (wt-%)	Brazing Temperature (°C)	No Detectable Leak in F19 Specimens (% NDL)	Average F19 Tensile Strength (MPa)	One Standard Deviation of Average (MPa)
94(a)	Au-18Ni (baseline)	1000	100	92.6	9.7
94	Au-Ni-Mo-1V	1000	71.4	95.8	15.7
94	Au-Ni-Mo-1V	1020	71.4	99.8	13.3
94	Au-Ni-Mo-2V	1000	85.7	103.4	3.7
94	Au-Ni-Mo-2V	1020	85.7	99.8	22.1
94	Au-Ni-Mo-3V	1000	85.7	85.4	12.8
94	Au-Ni-Mo-3V	1020	100	102.6	5.7
99.8	Au-Ni-Mo-1V	1000	14.3	61.3	16.0
99.8	Au-Ni-Mo-1V	1020	57.1	55.2	20.7
99.8	Au-Ni-Mo-2V	1000	85.7	35.2	14.6
99.8	Au-Ni-Mo-2V	1020	85.7	25.0	17.4
99.8	Au-Ni-Mo-3V	1000	85.7	70.1	13.5
99.8	Au-Ni-Mo-3V	1020	100	95.3	2.6

(a) Mo-Mn/Ni metallized surface finish (baseline process).

Hermeticity and Tensile Test Results

The brazed ASTM F19 tensile specimens were used to evaluate joint hermeticity and tensile strength; the results are summarized in Table 3.

Approximately 80% of the brazed 94%-alumina tensile specimens were hermetic. The criteria for hermeticity was defined as a leak rate less than 1.0 x 10^{-9} cm^3/s (std. helium atmosphere). The test specimens that "failed" had a leak rate of 10^{-7} to 10^{-4} cm^3/s (standard helium atmosphere). These leaks were attributed to microcracks in the alumina near the braze interface or insufficient braze material through the annular joint, where misalignment of the top piece in some of the specimens produced a tapered joint. Similar leak results were obtained for the 99.8% alumina tensile specimens. The 99.8% alumina samples that were brazed with the 1% vanadium alloy had the greatest dropout due to leaks.

The formation of braze balls at the joint's free surface (Fig. 4) also affected joint hermeticity. These discrete, local features were observed only on the 99.8% alumina tensile specimens, usually one specimen per data set. The leak distribution for these specimen was generally mixed, with both leakers and nonleakers. As with the braze droplets on the wetting samples, the braze balls concentrated high residual stresses in the ceramic that can initiate fine cracks (Fig. 4), which are then potential leak paths. Even with a hermetic joint, these stress-induced defects can affect the joint's mechanical strength. Their presence can be minimized by controlling the braze volume, joint clearance, applied load, processing conditions and interfacial reactions.

Tensile test results were dependent on the type of alumina, brazing filler metal composition and the brazing temperature (Table 3). The most consistent results were obtained with the 94% alumina specimens. Their tensile strength was nominally in the 95–100 MPa (13.8–14.5 ksi) range, compared with that of the metallized, "baseline" samples, 93 MPa (13.5 ksi). The only data set that fell below this range was for the samples brazed with the 3% vanadium composition at 1000°C. These samples failed at 85 MPa (12.3 ksi), suggesting a possible brazing temperature effect on strength for the higher vanadium-containing filler metal. Failure locations varied for the 94% alumina specimens, but most showed a mixture of substrate (ceramic) and braze failure. There was a slight preference (~60%) for failure to be associated with the bottom braze interface or ceramic.

The tensile strength of the 99.8% alumina specimens had a larger stress range, which was clearly influenced by the brazing temperature and ABA composition. The strength was generally lower than that obtained with the 94%-alumina material. The samples brazed with the 1% vanadium ABA yielded intermediate tensile values, with a nominal average strength of 58 MPa (8.4 ksi). At both brazing temperatures, the standard deviation of specimen strengths exceed 25% of the average.

Strength of the 99.8% alumina samples brazed with the 2% vanadium ABA was significantly lower than those that were brazed with the 1 and 3% vanadium-containing filler metals. The average tensile strength of the 1% specimens brazed at 1020°C was 25 MPa (3.6 ksi), well below the typical baseline strength for similar metallized alumina specimens. The 1000°C strength was slightly higher, with an average value of 35 MPa (5.1 ksi).

Finally, the 99.8% alumina specimens, brazed with the 3% vanadium ABA, produced a joint strength closest to the 94% alumina tensile values. The 1000°C samples failed at 70 MPa (10.2 ksi), while the 1020°C specimens failed at 95 MPa (13.8 ksi).

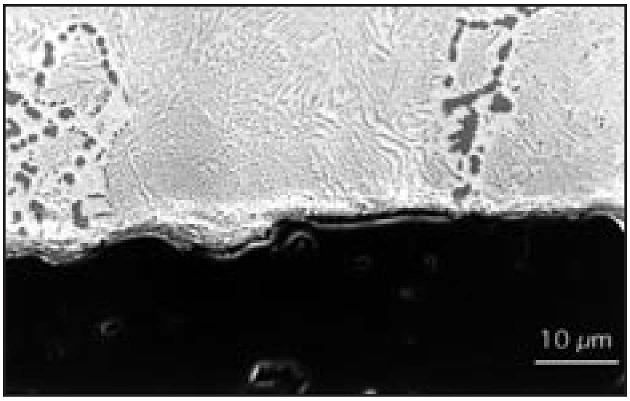

Fig. 6 — Cross section of a 99.8% Al_2O_3 sample brazed with the Au-Ni-Mo-2V alloy at 1000°C, showing intermittent bonding along the metal-ceramic interface.

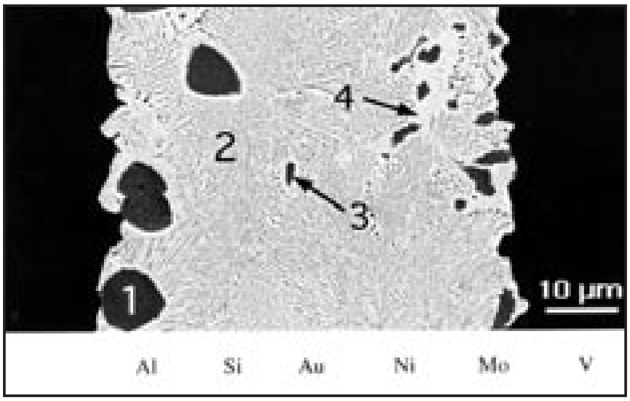

Fig. 7 — Microstructure and phase compositions (wt-%, EDS analysis) for a 94% Al_2O_3 braze joint that was fabricated with the Au-Ni-Mo-2V braze alloy at 1000°C. The top half of the braze specimen is observed on the left side of the image.

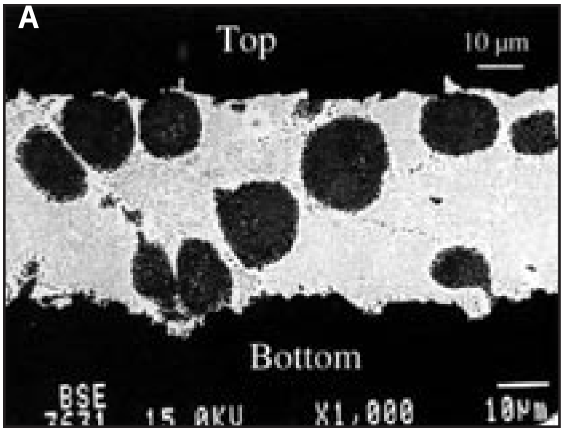

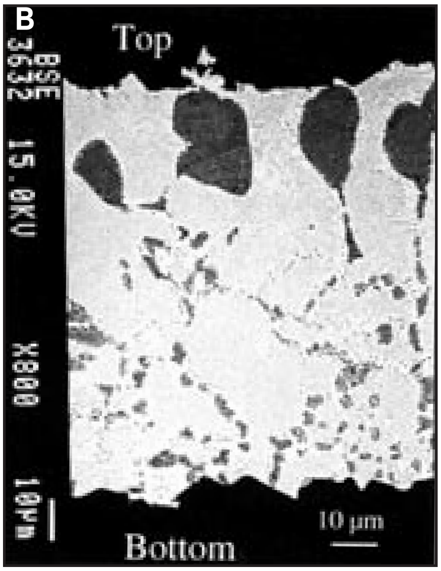

Fig. 8 — Microstructural comparison between (A) thin and (B) thick areas of a tapered 94% Al_2O_3 braze joint that was fabricated with the Au-Ni-Mo -3V alloy at 1000°C.

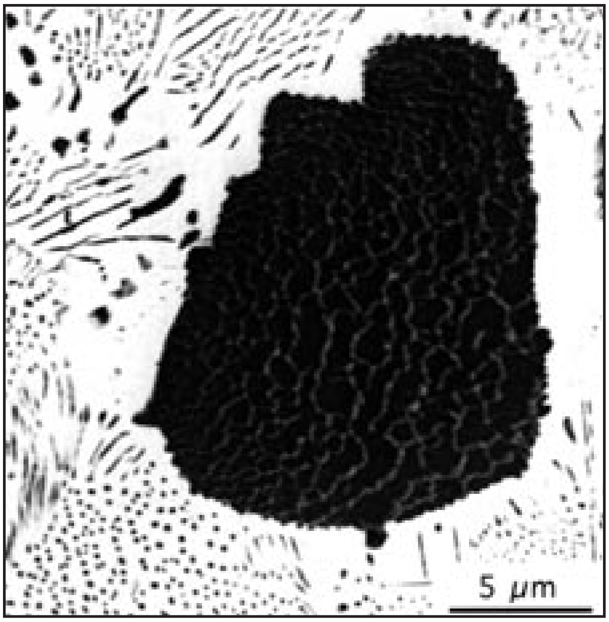

Fig. 9 — High-magnification back scattered electron image of the nickel-rich particles shown in Fig. 8 that reveals nonuniform distribution.

Table 4 — Composition and Volume Fraction of Ni-Rich Particles in 99.8% Al_2O_3 Braze Joints

Braze Joint (% V)	Braze Temp. (°C)	Composition (wt-%) Au	Mo	Ni	V	Volume Fraction
1 (1.0 V)	1000	36.1	7.3	49.1	9.0	0.083
	1020	34.9	8.3	48.6	8.8	0.129
2 (1.8 V)	1000	29.2	9.9	55.6	7.0	0.132
	1020	27.7	10.2	52.9	6.8	0.127
3 (2.9 V)	1000	26.5	12.0	57.7	4.7	0.140
	1020	25.8	13.7	57.7	4.4	0.140
{2.1 V(a)	n/a	10.9	7.2	72.9	9.8	0.260}

(a) Analysis of bulk Au-Ni-Mo-V braze alloy from Stephens and Hamann, Ref. 30.

The 99.8% alumina specimens failed primarily at the bottom metal-ceramic interface, with occasional fracture occurring in the bottom ceramic piece. Nearly 70% of the failures were along this lower braze interface.

Microstructural Analysis

Cross sections of the 94% alumina brazed tensile specimens revealed structures similar to those shown in Fig. 5. Joints were typically 60–80 microns (0.002–0.003 in.) wide and porosity-free, with several phases distributed throughout the microstructure. The braze maintained continuous, uninterrupted contact with the alumina substrate along the entire braze interface. The 99.8% alumina specimens contained identical microstructural features, although there were localized regions along the braze interfaces where slight separations were found between the metal and alumina — Fig. 6. Large globular features (dark particles in Fig. 5) were observed in the upper half of each joint; the remainder of the microstructure consisted of large, two-phase grains separated by finer particles.

The chemical composition of the various constituents in one specimen, obtained by wavelength-dispersive spectroscopy (WDS), is shown in Fig. 7. The large globular particles (Point 1) were found to be nickel-rich, and they contained the majority of the molybdenum in the joint. Their composition suggests these particles have a lower density than the remainder of the joint, which is consistent with their preferential distribution toward the top interface. The smaller dark particles (Point 3), distributed at boundaries between gold-rich grains, also contained a high-nickel content, but only small amounts of molybdenum.

The nickel-rich particles exhibited an interesting distribution throughout the various joints. Some of the tensile specimens, due to load imbalance or misalignment during brazing, produced joints with variable braze thickness. Examination of these tapered joints revealed a nearly uniform spatial distribution of the globular phase (as opposed to the local compositional volume fraction) across the thin (25 µm) and thick (125 µm) areas of the joint — Fig. 8. Since the initial thickness of the braze alloy (foil) was uniform, these results suggest the lower-density, nickel-rich particles form during melting and solidification of the filler metal and segregate to the upper region of the higher-density, gold-rich phase in the wider braze gaps.

Examination at higher magnification reveals the nickel-rich particles are not a single phase but rather a textured structure with nonuniform composition —

Table 5 — Al-V-O Structures Identified as Possible Reaction Layer Compounds Based upon X-Ray Diffraction Data

Compound	PDF No.	Crystal Type	d-spacing (nm)
$AlVO_3$	25–0027	cubic	0.487
AlV_2O_4	25–0025	tetragonal	0.484
AlV_2O_4	25–0026	cubic	0.472

Fig. 9. Average composition of these particles (Table 4) varied with both filler metal composition and brazing temperature but was independent of the ceramic substrate. The compositional data suggest a (Au, Mo, V)$Ni_{2 \text{ or } 3}$ compound.

Examination of the 94% alumina fracture surfaces revealed large areas of transgranular ceramic failure — Fig. 10A. However, in many cases the fracture path traversed across the braze joint several times, resulting in substrate failures on both sides of the joint. The transition regions typically revealed localized intergranular ceramic failure, as shown in Fig. 11. At these locations, the braze metal remained well bonded to the ceramic, with ductile failure of the gold-rich phase and limited deformation of the darker, nickel-rich areas.

Conversely, the 99.8% alumina fractures were dominated by failures at the metal-ceramic interface, with the fracture path almost exclusively proceeding along a single ceramic interface. The limited areas of ceramic substrate failure exhibited substantial intergranular failure of the alumina — Fig. 10B. Far more common was the fracture appearance shown in Fig. 12, where the braze appears to be separated cleanly from the ceramic. The resulting metallic surfaces show almost no deformation, and the individual constituents of the braze joint are clearly visible.

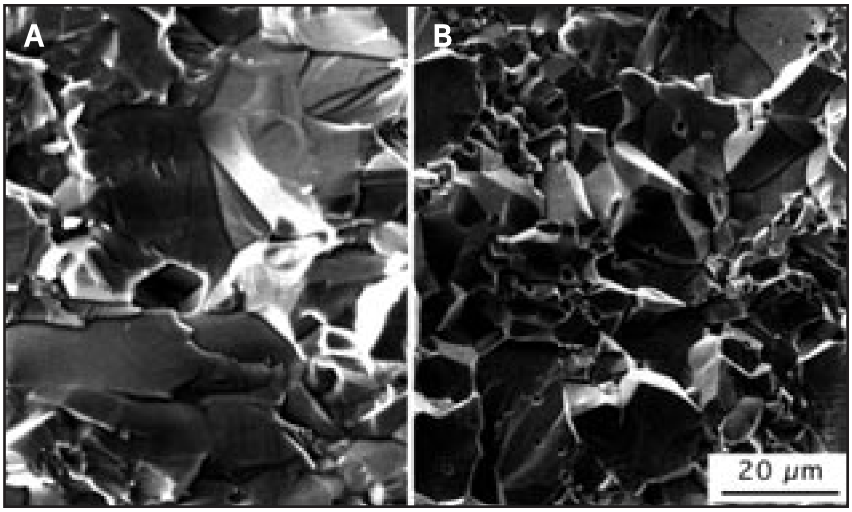

Fig. 10 — Fracture surfaces of brazed alumina tensile specimens that demonstrate a generally transgranular fracture mode in the 99.8% Al_2O_3 (A, left) and intergranular fracture mode in the 94% Al_2O_3 (B, right) specimens.

No interfacial reaction layer was observed using optical or scanning electron microscopy (SEM). However, transmission electron microscopy (TEM) revealed a very thin layer of material at the metal-ceramic interface. This layer, which appears rippled in Fig. 13, was found at several but not all locations examined on both 94 and 99.8% alumina specimens. These features, situated between the alumina grains and the braze metal (both gold-rich and nickel-rich phases) typically measured about 20–30 nm (0.8–1.2 μin.) at the widest point.

Higher magnification views of the interface region between the metal and ceramic are shown in Fig. 14. A narrow (approximately 20 nm thick) reaction layer was identified at the interface. From electron diffraction and Fourier analysis of the observed lattice fringes, the orientation of the alumina grain was determined to be along a <1101> type zone. Using the alumina lattice fringes as an internal calibration, the spacing of the horizontal lattice fringes observed in the interfacial layer was measured to be 4.8 angstroms. This spacing is consistent with the 4.84-angstrom spacing measured from a selected-area electron diffraction pattern, also taken from the interfacial region.

EDS analysis of the interfacial region

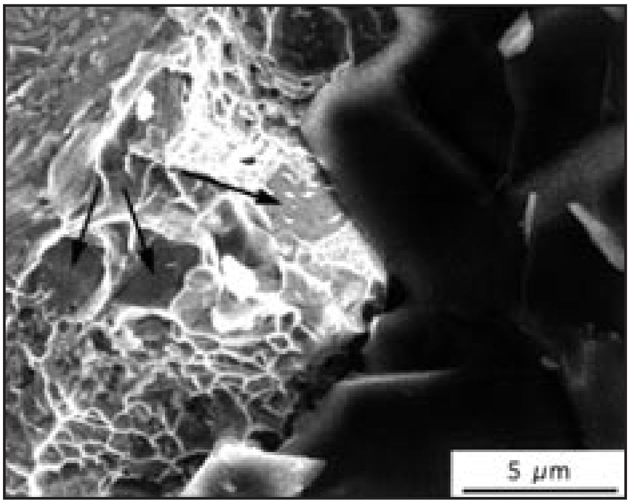

Fig. 11 — Regions of braze metal failure in the 94% Al_2O_3 tensile specimens that indicate a ductile fracture mode in the gold-rich areas and limited deformation of the nickel-rich particles (arrows).

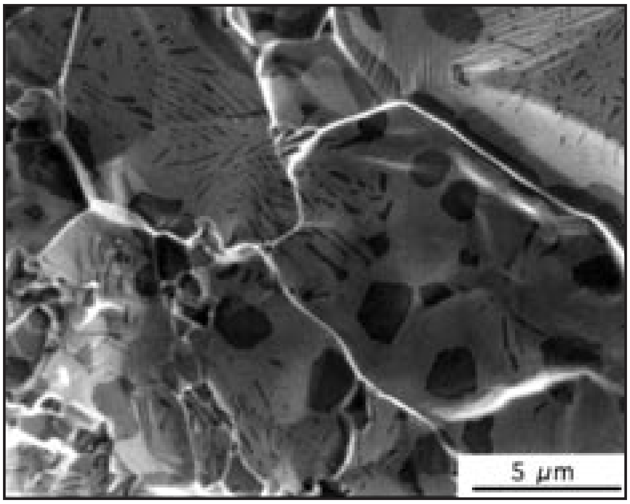

Fig. 12 — Fracture surface of a 99.8% Al_2O_3 tensile specimen that failed along the braze metal-ceramic interface. The exposed metallic surface shows almost no deformations.

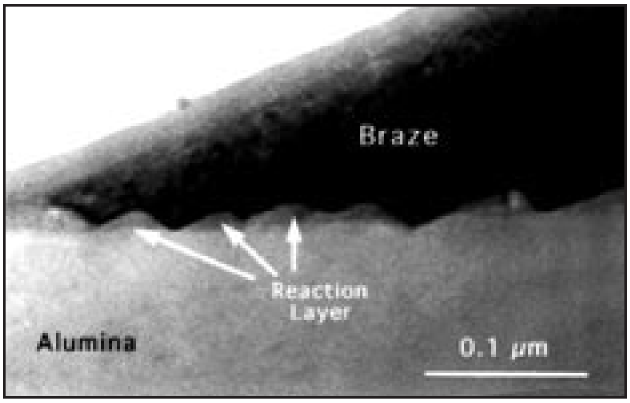

Fig. 13 — TEM image of the braze metal-alumina interface; the reaction layer has a rippled appearance.

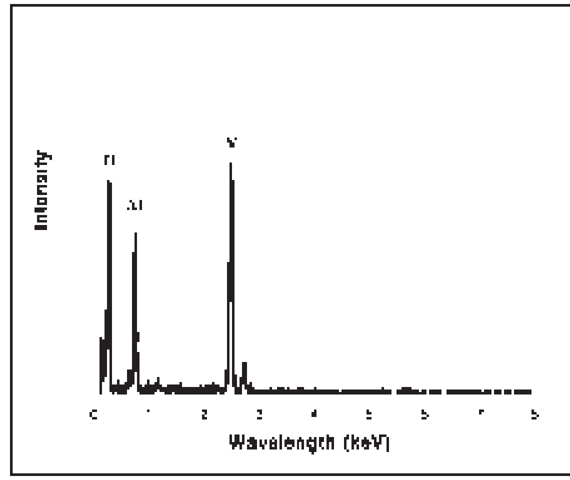

Fig. 15 — X-ray spectrum of the braze metal-alumina reaction layer shows the presence of oxygen, aluminum and vanadium.

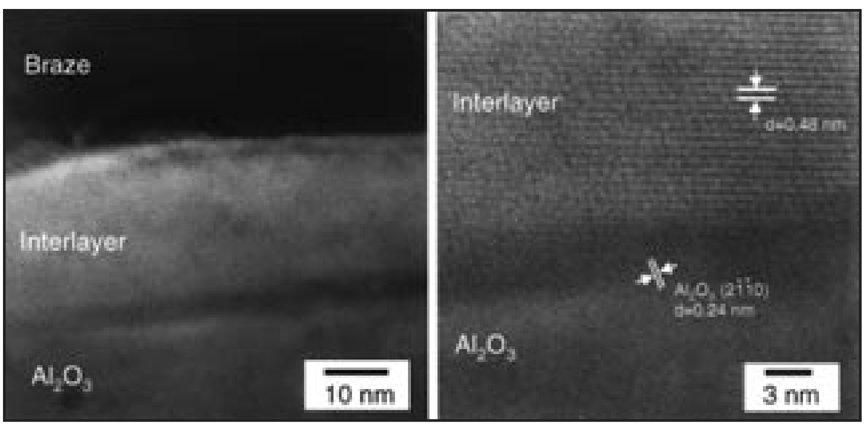

Fig. 14 — HRTEM image of the braze metal-alumina interface that was used to obtain lattice parameters of the brazing reaction product.

(Fig. 15) indicated only oxygen, vanadium and aluminum were present; no gold, nickel or molybdenum (or silicon in the 94% alumina samples) was detected. To identify the phase of the interfacial layer, the interplanar angles and spacings measured from a selected-area diffraction pattern obtained from the interfacial layer were compared against diffraction data listed in the Powder Diffraction File (PDF) database for compounds of vanadium-oxygen, vanadium-oxygen-aluminum, vanadium-aluminum and elemental vanadium.

The analysis eliminated the majority of the compounds from further consideration on the basis of inconsistent d-spacings and/or interplanar angles. Only for vanadium-oxygen-aluminum compounds were matches obtained with the observed diffraction pattern. Specifically, three compounds (Table 5) including a cubic phase of $AlVO_3$ and cubic and tetragonal phases of AlV_2O_4 have reported structures that are consistent with the experimental diffraction pattern. Each of these phases matches the observed diffraction pattern quite well; the calculated and measured interplanar angles are within 1 deg and the measured d-spacings are all consistent to within about 3%.

All three phases are closely related structurally. The powder diffraction file describes both cubic phases as spinel structures; typically, a spinel has a formula type of AlB_2O_4. The PDF also describes $AlVO_3$ as a metal-deficient spinel. With the present diffraction data, it is not possible to further distinguish between these three structures.

Discussion

Microscopic Considerations

The binary Au-18Ni (BAu-4) composition does not wet alumina substrates. Generally, this lack of wettability can be attributed to the nature of atomic bonding (either ionic or covalent) in ceramics that lack the delocalized bonding electrons found in metals (Ref. 15). Alumina atomic bonds have strong ionic characteristics compared with other ceramics of engineering interest, particularly nonoxides such as Si_3N_4 and SiC. Consequently, a braze alloy must have a high oxidation potential to generate the chemical reaction(s) necessary to wet alumina. Small additions of titanium to several face-centered-cubic elements (Cu, Ni, Au) have been shown to facilitate wetting on alumina through the formation of a titanium-oxide reaction layer (Refs. 16–18). Vanadium is a less-potent oxidizing agent than titanium. Thus reduction of alumina by vanadium-containing braze alloys is more difficult, as evidenced by the unfavorable free-energy values for simple oxide reactions. Thermodynamic data for more complex systems, such as the spinel-type compounds, indicated by the diffraction results, are not readily available. However, electron microscopy results suggest the reaction layer is either nonexistent or extremely thin (undetectable) in many areas.

Since the braze alloy was preplaced, no flow or wetting was required to “fill” the joint. Previous investigators (Refs. 19, 20) have suggested mechanisms for time-dependent formation of a reaction product, where the reaction layer forms at multiple, isolated locations at the braze-ceramic interface. These islands can, over time, grow laterally as the reaction progresses, eventually leading to complete convergence. In the areas between the islands of reaction product, the braze alloy appears to be at least weakly bonded directly to the alumina substrate. Previous researchers (Refs. 21, 22) have found both gold and nickel can adhere to

Al_2O_3, although bond strengths are below the strength of the ceramic. Bogicevic and Jennison (Ref. 23) suggest a partial monolayer of metal atoms can bind strongly to alumina through ionic bonding. However, at a thickness greater than one monolayer, the nature of the alumina-metal bond changes from ionic to electrostatic, with a drastic decrease in bond strength. It seems likely the metal-ceramic interface in tensile specimens fabricated in the current study possess a mixture of well bonded metal (facilitated by the AlV_2O_4 or $AlVO_3$ reaction product) and areas of weak bonding. The tensile results suggest the 94% alumina specimens contain a larger percentage of strongly bonded regions than the high-purity specimens.

Both the nucleation and growth rate of the reaction layer may be affected by crystallographic orientation of the individual Al_2O_3 grains. Previous studies found a large variation in calculated surface energy as a function of orientation for ionic crystals (Refs. 24, 25), in contrast with metallic crystals where surface energies are much more isotropic.

In the current study, brazing time was held constant. While the reaction layer appeared to be discontinuous in both 94 and 99.8% alumina specimens, the strength of the 94% specimens was clearly superior. Assuming the individual grains of alumina have essentially the same composition and a random orientation in both ceramic substrates, then the primary difference in bond strength appears to be related to the presence of the glass-grain boundary phase present in the 94% specimens. As previously noted, SiO_2 has marginal thermodynamic stability in the presence of vanadium at the brazing temperature. Furthermore, at 1000°C, SiO_2 is reduced in a hydrogen atmosphere having a dew point of approximately –80°C, only slightly drier than the environment used for these experiments. Small quantities of silicon were detected in the braze joints of the 94% specimens (Fig. 7), evidence of some reduction of SiO_2 during brazing.

The presence of the glassy grain boundary phase could contribute to the improved strength of the 94% specimens by several mechanisms. Since the glass phase represents approximately 8 vol-% of the specimen, the surface area of alumina exposed to the molten braze alloy is reduced accordingly.

Secondly, following the air-firing step, a very thin layer of silicon-rich material, approximately 10 angstroms or less thick (Ref. 26), covers or partially covers the newly exposed (machined) surfaces. This coverage, in addition to the original 8% surface component, may facilitate wetting and possibly reduce the time necessary for nucleation of the reaction layer.

Finally, the reduction of SiO_2 by vanadium, or by hydrogen, would lead to the presence of either free silicon or oxygen in the molten braze filler. These compositional changes may influence the thermodynamic activity of vanadium in the braze alloy, thus changing the growth kinetics of the interface reaction product. Similarly, silicon or oxygen in the molten filler may also act as a catalyst for the reaction, although no silicon was detected in the reaction layer at the metal-ceramic interface. Traces of silicon were found in the joint.

Macroscopic Considerations

Solidification of binary Au-Ni alloys occurs as a single-phase, solid solution. However, at lower temperatures (below 700–800°C) this structure becomes unstable, and, if the cooling rate is sufficiently low, a phase separation will occur resulting in nickel-rich and gold-rich phases (Ref. 27).The presence of a small amount of Mo in these braze alloys is thought (Ref. 28) to stabilize an additional phase (which facilitates mechanical working of the alloys in production). As previously noted, the compositions of the braze filler metals examined in this study appear to have extended phase instability at temperatures close to their liquidus temperatures. These results are consistent with those of Kang and Kim (Ref. 29), who detected two discrete melting events in experimental two-phase Au-Ni compositions containing Mo, Fe and Cr additions. Stephens and Hamann, in studies of bulk samples of the commercial Au-15Ni-0.7Mo-2.1V alloy (Ref. 30), identified chemical compositions of two phases from samples annealed at 910°C and then water quenched. The composition of the Ni-rich phase in the bulk alloy is included for comparison with the brazed specimens (Table 4). Note the volume fraction of the Ni-rich, vanadium-containing equilibrium phase in the bulk material (Ref. 30) is relatively high compared to that found in the actual braze joints. The difference was attributed to the presence of small amounts of vanadium and molybdenum in the gold-rich regions and the eutectic constituent of the braze joint — Fig. 7.

The propensity for tensile specimen failures to be associated with the lower metal-ceramic interface may be explained by several factors. The nickel (and vanadium) rich globular phases are preferentially distributed toward the top of the joint — Fig. 5. Since vanadium is fundamentally involved in the reaction with the ceramic substrate, a higher vanadium concentration toward the top of the joint (found in a lower-density liquid phase) could result in a more developed reaction product (higher percentage) along this upper interface. Additionally, the globular phases contain the majority of the molybdenum and vanadium content of the filler material; these elements possess a lower coefficient of thermal expansion than either gold or nickel. Thus, the presence of the globular phase may locally reduce the thermal expansion coefficient of the braze alloy near the metal-ceramic interface, thereby diminishing the residual stresses near that interface.

Finally, the data on temperature distribution along tensile specimens indicated heat was preferentially extracted from the top piece of the braze specimen during cooling. Consequently, the temperature gradient imposed on the braze joint could cause the liquid filler metal to solidify from the top ceramic interface (either from the reaction layer or from the alumina substrate) toward the bottom interface. The solidifying metallic phases, either Ni- or Au-rich, would have nucleated on the ceramic structure at the upper solid-liquid interface, with some preferential crystallographic orientation.

Conclusions

The brazing studies conducted on polycrystalline alumina specimens in the current investigation have led to an understanding of some of the factors that determine mechanical and microstructural behavior when using Au-Ni-Mo-V filler metals. The following conclusions are drawn from the results of this work:

1) Au-15.5Ni-0.7Mo-based filler metals containing 1, 2 or 3% vanadium exhibit limited wetting on either 94 or 99.8% alumina substrates at temperatures of 1000 and 1020°C for 5 min in a dry hydrogen atmosphere. All filler metals showed a preferential tendency to wet the glassy phase found in the 94% alumina specimens.

2) Specimens made of 94% alumina showed consistently high strength and acceptable hermeticity after being brazed with the three ABA filler metals at the two brazing temperatures. Tensile fractures generally occurred in the ceramic substrate.

3) High-purity 99.8% alumina specimens yielded hermetic joints when brazed with the 2 and 3% vanadium filler metals. However, their joint strength was generally lower than comparable 94% alumina braze specimens. The 1% vanadium-containing alloy yielded good tensile values, intermediate to the 1 and 3%

vanadium filler metals, but produced significantly more joint leaks. The 99.8% alumina specimens brazed with the 2% vanadium alloy yielded the poorest tensile properties. Only the 3% vanadium composition yielded joint strengths approaching the 94% alumina values. The fracture paths in the 99.8% alumina specimens occurred across the metal-ceramic interface.

4) A reaction layer, which appears to be discontinuous, was observed at the metal-ceramic interface. The larger structure was tentatively identified as either a AlV_2O_4 or a $AlVO_3$ spinel.

5) Differences in joint strength between the two types of alumina can be attributed to the presence of a greater amount of glassy grain boundary binder phase present in the 94% alumina ceramic. Small amounts of Si were found in the braze microstructure of these specimens, indicating some dissolution or dissociation of SiO_2 during brazing. No evidence was found to identify conclusively the mechanism for the greater strength in the 94% alumina specimens.

6) Tensile failures were more likely to be associated with the lower metal-ceramic interface, where joint solidification probably occurred last due to the thermal gradient imposed during cooling from the peak brazing temperature. The resulting reactions and structure favor a stronger top interface.

Acknowledgments

The authors would like to acknowledge the contributions of Ronnie Albers, Tom Crenshaw, Celeste Drewian, Tom Headley, Paul Hlava, Alice Kilgo, Doug Medlin and Gary Zender to the project. The work was supported by the U. S. Department of Energy's Defense Programs and Sandia's Research Foundations Program.

References

1. Mizuhara, H., and Mally, K. 1985. Ceramic-to-metal joining with active brazing filler metal. *Welding Journal* 64(10): 27–32.

2. Mizuhara, H., Huebel, E., and Oyama, T. 1989. High-reliability joining of ceramic to metal. *Ceramic Bulletin* 68(9): 1591–1599.

3. *Brazing Handbook*, 4th Edition. 1991. Ceramic brazing. AWS, Miami, Fla., pp. 411–422.

4. Mizuhara, H., and Oyama, T. 1993. Ceramic/metal seals. *ASM Handbook*, Vol. 4, pp. 502–510.

5. Hosking, F. M., and Koski, J. 1992. Graphite-metal brazing for thermal applications. *TMS Metal Science of Joining Symposium Proceedings*, pp. 307–314.

6. Selverian, J. H., Ohuchi, F. S., and Bortz, M. 1991. Interface reactions between titanium thin films and sapphire. *Journal of Materials Science* 26(23): 6300–6308.

7. Selverian, J., and Kang, S. 1992. Interactions between Ti and alumina-based ceramics. *Journal of Materials Science* 27(16): 4536–4544.

8. Santella, M. L., and Pak, J. J. 1993. Brazing titanium-vapor-coated zirconia. *Welding Journal* 72(4): 165-s–172-s.

9. Moorehead, A. J., Elliott, W. H., and Kim, H.-E. 1993. Brazing of ceramic and ceramic-to-metal joints. *ASM Handbook*, Vol. 6, pp. 948–960.

10. Stephens, J. J., Vianco, P. T., and Hosking, F. M. 1996. The active metal brazing of TZM-Mo and SiN ceramics. *Journal of Metals* 48(1): 54–58.

11. Tillmann, W., Lugscheider, E., Schlimbach, K., Manter, C., and Indacochea, J. E. 1998. Heat-resistant active brazing of silicon nitride part 2: metallurgical characterization of the braze joint. *Welding Journal* 77(3): 103-s to 109-s.

12. Adamson, A. W. 1990. *Physical Chemistry of Surfaces*. John Wiley & Sons, Inc., pp. 28–36 and 379–420.

13. Humpston, G., and Jacobson, D. M. 1994. *Principles of Soldering and Brazing*. ASM International, Materials Park, Ohio, pp. 9–12.

14. American Society for Testing and Materials (ASTM).1996. Standard test method for tension and vacuum testing metallized ceramic seals. *1996 Annual Book of ASTM Standards*, Designation F19-64 (1995)e1, Vol. 10.04, pp. 25–28.

15. Pauling, L. 1939. *The Nature of the Chemical Bond*. Cornell University Press, Ithaca, N.Y.

16. Loehman, R., and Tomsia, A. 1988. Joining of ceramics. *Ceramic Bulletin* 67(2): 375–380.

17. Moorhead, A. J. 1987. Direct brazing of alumina ceramics. *Advanced Ceramic Materials* 2(2): 159–166.

18. Kristalis, P., Drevet, B., Valignot, N., and Eusthathopoulos, N. 1994. Wetting transitions in reactive metal/oxide systems. *Scripta Metallallurgica et Materialia* 30(9): 1127.

19. Landry, K., and Eustathopoulos, N. 1996. Dynamics of wetting in reactive metal/ceramic systems: linear spreading. *Acta Metallurgica* 44(10): 3923–3932.

20. Meier, A., Chidambaram, P. R., and Edwards, G. R. 1998. Modelling of the spreading kinetics of reactive brazing alloys on ceramic substrates: copper-titanium alloys on polycrystalline alumina. *Acta Materialia* 46: 4453–4467.

21. Klomp, J. T. 1972. Bonding of metals to ceramics and glasses. *Ceramic Bulletin* 51(9): 683.

22. Crispin, R. M., and Nicholas, M. G. 1976. The wetting and bonding behavior of some nickel alloy-alumina systems. *Journal of Materials Science* 11: 17–21.

23. Bogicevic, A., and Jennison, D. R. 1998. Variations in the nature of metal adsorption on ultrathin Al_2O_3 films. *Phys. Rev. Lett.* 82(20): 4050–4053.

24. Tasker, P. W., and Duffy, D. M. 1984. The structure and properties of the stepped surfaces of MgO and NiO. *Surface Science* 137: 91–102.

25. Tasker, P. W. 1984. *Structure and Properties of MgO and Al_2O_3 Ceramics*. American Ceramic Society, Columbus, Ohio, pp. 176–189.

26. Unpublished Auger Electron Spectroscopy (AES) data, Sandia National Laboratories, 1998.

27. Massalski, T. B. 1987. *Binary Alloy Phase Diagrams*. ASM International, Materials Park, Ohio.

28. Mizuhara, H. 1999. Private communication.

29. Kang, S., and Kim, H. J. 1995. Design of high-temperature brazing alloys for ceramic-metal joints. *Welding Journal* 74(9): 289-s to 295-s.

30. Stephens, J. J., and Hamann, K. D. 1995. The effect of vanadium active metal addition on the mechanical properties of a nickel-gold braze alloy. Presented at 124th TMS Annual Meeting, Las Vegas, Nev.